ELSEVIER

Chemical Engineering Journal 122 (2006) 149–157

Chemical Engineering Journal

www.elsevier.com/locate/cej

Xylene isomerization in a membrane reactor Part II. Simulation of an industrial reactor

Andrea L. Deshayes [a], Eduardo E. Miró [a,*], Gabriel I. Horowitz [b]

[a] *Instituto de Investigaciones en Catálisis y Petroquímica (FIQ, UNL-CONICET), Santiago del Estero 2829, 3000 Santa Fe, Argentina*

[b] *Repsol-YPF, Baradero S/N, Ensenada, Buenos Aires 1925, Argentina*

Received 10 March 2006; received in revised form 7 June 2006; accepted 13 June 2006

Abstract

A model and the simulation of a membrane reactor for xylene isomerization are presented. Kinetic parameters for the reaction carried out under industrial conditions are optimized using plant data with a conventional plug-flow model. In the membrane reactor, the characteristics of a ZSM-5 film supported on porous SS tubes, which was developed in our laboratory, are included to simulate the improvement in *p*-xylene production at 370 °C. The values used for the simulations correspond to ternary mixtures at 370 °C, and they are: 4.70×10^{-8}, 8.44×10^{-9} and 8.45×10^{-9} mol s^{-1} m^{-2} Pa^{-1} for *p*-, *o*- and *m*-xylene, respectively. In this vein, while for the output of the conventional plug-flow reactor the ratio *p*-/*o*-/*m*-xylene is 1.000/0.936/1.940, in the case of the membrane reactor the rate is improved to 1.000/0.830/1.719, taking into consideration the contribution of the permeate and retentate sides. Consequently, an increase of 12% in *p*-xylene production is predicted by increasing permeation area and sweep gas flow, restricted to a reasonable pressure drop and whithin the physical and constructive feasibility of the SS tubes.

Keywords: Xylene isomerization; Industrial reactor; Membrane reactor; Simulation

1. Introduction

In the last decades there has been a tendency towards energy saving in order to optimize production costs as well as an increasing interest in environmental issues. This has promoted the study of new separation technologies, since conventional separation operations usually demand large amounts of energy. The *p*-xylene production is one of the processes in which a great deal of energy is used in the separation and purification stages. This has led both public organizations and private companies to support research and development on microporous membranes that allow the separation of *p*-xylene from a xylene mixture.

The most common technology used to carry out this operation involves both the separation of *o*-xylene by distillation and of *m*-xylene by crystallization. Not only could the use of membranes for *p*-xylene separation have a strong environmental advantage, but it may also have an economic impact over the whole process.

There exist many materials for the preparation of microporous membranes that allow for transport mechanisms (adsorption–diffusion and molecular sieving) appropriate for achieving separations. Zeolites, with their regular structure, resistance to acids, thermal stability, feasibility of steady state operation, low energetic consumption, great potential for combined systems of reaction/separation, are the microporous materials that have recently generated the most interesting, promising membranes [1–4].

Additionally, they present the advantage of being able to be modified by habitual techniques of chemical and physical deposition: ionic exchange, impregnation, etc.

Zeolitic membranes are formed by a zeolite (ZSM-5, mordenite, MFI, etc.) supported on a macro or mesoporous material (alumina or stainless steel). They allow the separation of gases or vapours with different kinetic diameter by molecular sieving. For instance, separations of *n*-butane/*i*-butane, *n*-hexane/2-2-dimethylbutane, methanol/methyl-*tert*-butyl-ether, *p*-xylene/*o*-xylene and *m*-xylene mixtures [2].

p-Xylene is of great commercial interest, since fibers and several polymers can be obtained from it. Its effective separation from a C8 aromatic mixture is, therefore, of enormous relevance.

* Corresponding author. Tel.: +54 342 4536 861; fax: +54 342 4536 861.
E-mail address: emiro@fiqus.unl.edu.ar (E.E. Miró).

1385-8947/$ – see front matter © 2006 Elsevier B.V. All rights reserved.
doi:10.1016/j.cej.2006.06.010

A commercial reactor is modeled as a single stage, adding the presence of a membrane whose features allow the separation of the desired compound. By comparing the two models, it is possible to estimate the benefits brought about by the membrane in order to achieve the reactor optimization and assess the economic advantages of this technology.

This article is aimed to analyze the improvement introduced by the membrane synthesized in the first part of this work in the performance of a commercial reactor. Additionally, the influence of different variables such as permeation area and sweep gas flow rate in the reactor's operation is also studied.

2. Isomerization kinetics

It has been shown that for the xylene isomerization in heterogeneous systems, the most efficient catalysts are those that contain silica–alumina, silica–magnesia and silica–alumina–zirconia [5]. They are acid catalysts that promote aromatic restructuring. If there is also ethylbenzene in the mixture, high pressures and metal/silica–alumina bifunctional catalysts are used. The metal introduces a hydrogenating function and, for the case of Ni on silica–alumina, the metal helps to control the deactivation, by removing carbonous material deposited on the surface. The isomerization over this kind of catalyst proceeds according to the following scheme [6–9]:

o-xylene $\leftrightarrow$ *m*-xylene $\leftrightarrow$ *p*-xylene

Meanwhile, the kinetics takes the form of:

$$r_i = \frac{k_i K_i P_i}{1 + \sum K_j P_j} \quad (1)$$

The kinetic equation shows that the reaction on one catalyst site is the rate-determining step.

In industrial conditions, the presence of ethylbenzene and other aromatic compounds in the mixture entering the reactor, together with the use of hydrogen as a carrier also provoke side reactions such as hydrogenolysis, xylene and toluene disproportionation, and ethylbenzene isomerization. The introduction of hydrogen to the reactor feed suppresses side reactions and coke formation, and increases the reaction rate [10].

3. Reaction modeling

The equations used for the modeling of both the commercial reactor as it is currently functioning and a membrane reactor that uses the same catalyst load will be discussed below. The adopted nomenclature is shown in Table 1, as well as some of the constant values employed.

3.1. Reaction rates

During the xylene isomerization reaction, due to the presence of other aromatics and hydrogen in the system, a number of side reactions occur. Ethylbenzene suffers isomerization to xylenes, whereas the main side reactions can be divided into hydrogenolysis and disproportionation.

Table 1
Nomenclature

Symbol	Description	Value	Units
$A_{permeation}$	Area available for permeation		m^2
$A_{reactor}$	Total reactor section	10.75	m^2
A_t	Fixed-bed section		m^2
c_i	Molar concentration of species *i*		$kmol\ m^{-3}$
cp_g	Gas mixture heat capacity		$kcal\ kg^{-1}\ K^{-1}$
Cp_g	Gas mixture heat capacity		$kcal\ kmol^{-1}\ K^{-1}$
D_i	Effective permeability of species *i* through the membrane		$kmol\ h^{-1}\ m^{-2}\ atm^{-1}$
D_{part}	Catalyst particle diameter		m
E_{a_k}	Direct reaction activation energy		$kcal\ mol^{-1}$
$E_{a_{mk}}$	Inverse reaction activation energy		$kcal\ mol^{-1}$
G	Mass flux of the gas mixture		$kg\ h^{-1}\ m^{-2}$
$\Delta H_{reaction}$	Heat of reaction		$kcal\ mol^{-1}$
k_k	Direct reaction rate constant		$kmol\ kg_{cat}{}^{-1}\ h^{-1}\ atm^{-\beta}$
k_{mk}	Inverse reaction rate constant		$kmol\ kg_{cat}{}^{-1}\ h^{-1}\ atm^{-\beta}$
K_i	Adsorption equilibrium constant for the *i* xylene on the catalyst.		atm^{-1}
L_0	Total length of reactor		m
n	Number of membrane tubes in the membrane multitubular reactor		–
P	Total pressure		atm
P_i	Partial pressure of species *i*		atm
q_i	Molar flux of species *i*		$kmol\ h^{-1}\ m^{-2}$
q_{total}	Molar flux of the input gas mixture		$kmol\ h^{-1}\ m^{-2}$
Q_i	Molar flow rate of species *i*		$kmol\ h^{-1}$
Q_{sweep}	Sweep gas flow rate		$kmol\ h^{-1}$
r	Radius of each tube for the multitubular membrane reactor		m
r_i	Rate of reaction of species *i*		$kmol_i\ h^{-1}\ kg_{cat}{}^{-1}$
R_1	Inner radius of the membrane tube (or equivalent inner radius for a multitubular membrane reactor)		m
R_2	Plug-flow reactor radius	1.85	m
$S_{permeate}$	Permeate section		m^2
T	temperature		K
u_s	superficial velocity in the bed		$m_{gas}{}^3\ m_{section}{}^2\ h^{-1}$
y_i	Molar fraction of species *i*		$mol_i\ mol_{total}{}^{-1}$
z	Reactor length		m
Greek symbols			
β	Reaction order		–
ε	Porosity of the packed bed	0.37	$m_{gas}{}^3\ m_{total}{}^{-3}$
μ_{gas}	Viscosity of the gas mixture		$kg\ m^{-1}\ s^{-1}$
ν_i	Stoichiometric coefficient of species *I*		–
ρ_g	Gas mixture density		$kg\ m^{-3}$
ρ_{bed}	Catalytic bed density	620	$kg_{cat}\ m^{-3}$
Subscripts			
bz	Benzene		
ebz	Ethylbenzene		

Table 1 (*Continued*)

Symbol	Description	Value	Units
h	Hydrogen		
m	*m*-Xylene		
p	*p*-Xylene		
o	*o*-Xylene		
tmb	Trimethylbenzene		
tol	Toluene		
x	Xylene		
1, 2, 3, ...	Chemical reaction 1, 2, 3, ...		
Superscript			
′	Permeate side		

The kinetic expressions are shown in Table 2. They were obtained from the literature [6–11]. Corma et al. [6–9] studied this system thoroughly, so the kinetic parameters determined by them were used as starting values for our simulations, and then modified in order to describe the operation of the industrial reactor in an efficient way (Table 3).

3.2. Commercial reactor modeling

According to Froment and Bischoff [12], a fixed-bed reactor can be described by either a pseudo-homogeneous or a heterogeneous model. The commercial isomerization reactor is operated in a plug-flow mode, which has been corroborated numerically according to plant information. Reynolds numbers were estimated for several days of operation, being always bigger than 10^4. Peclet numbers for axial and radial dispersion were also calculated. The axial Peclet number was found to be 2, independent of the Reynolds number, which corroborates the plug-flow operation (Froment [13], Froment and Bischoff [12]). In addition, the ratio L_0/D_{part} is bigger than 50, so according to Carberry [14] the axial mixing can be neglected. The radial Peclet number was 10, which indicates that flow is well distributed in the radial direction of the commercial reactor.

Table 3
Adjusted kinetic parameters for the system of reactions

Parameter	Value	Units
k_{0_1}	2.89×10^6	kmol kg_{cat}^{-1} h^{-1}
$k_{0_{m1}}$	1.53×10^6	kmol kg_{cat}^{-1} h^{-1}
E_{a_1}	23.866	kcal mol^{-1}
$E_{a_{m1}}$	24.030	kcal mol^{-1}
k_{0_2}	2.57×10^3	kmol kg_{cat}^{-1} h^{-1}
$k_{0_{m2}}$	4.65×10^3	kmol kg_{cat}^{-1} h^{-1}
E_{a_2}	20.364	kcal mol^{-1}
$E_{a_{m2}}$	19.944	kcal mol^{-1}
K_p	1.237	atm^{-1}
K_o	0.477	atm^{-1}
K_m	1.333	atm^{-1}
k_{0_3}	3.40×10^2	kmol kg_{cat}^{-1} h^{-1} atm^{-2}
E_{a_3}	20.000	kcal mol^{-1}
k_{0_4}	5.62×10^2	kmol kg_{cat}^{-1} h^{-1} atm^{-2}
E_{a_4}	20.000	kcal mol^{-1}
k_{0_5}	2.92×10^1	kmol kg_{cat}^{-1} h^{-1} atm^{-2}
E_{a_5}	20.000	kcal mol^{-1}
k_{0_6}	1.91×10^{-4}	kmol kg_{cat}^{-1} h^{-1} atm^{-2}
E_{a_6}	−0.110	kcal mol^{-1}
k_{0_7}	5.49×10^3	kmol kg_{cat}^{-1} h^{-1} atm^{-1}
E_{a_7}	20.000	kcal mol^{-1}
k_{0_8}	4.34×10^3	kmol kg_{cat}^{-1} h^{-1} atm^{-2}
$k_{0_{m8}}$	1.25×10^3	kmol kg_{cat}^{-1} h^{-1} atm^{-2}
E_{a_8}	20.000	kcal mol^{-1}
$E_{a_{m8}}$	19.440	kcal mol^{-1}
k_{0_9}	6.98×10^1	kmol kg_{cat}^{-1} h^{-1} atm^{-2}
$k_{0_{m9}}$	5.46×10^2	kmol kg_{cat}^{-1} h^{-1} atm^{-2}
E_{a_9}	17.400	kcal mol^{-1}
$E_{a_{m9}}$	17.340	kcal mol^{-1}
$k_{0_{10}}$	1.08×10^5	kmol kg_{cat}^{-1} h^{-1} atm^{-2}
$k_{0_{m10}}$	1.16×10^5	kmol kg_{cat}^{-1} h^{-1} atm^{-2}
$E_{a_{10}}$	22.500	kcal mol^{-1}
$E_{a_{m10}}$	21.600	kcal mol^{-1}
$k_{0_{11}}$	5.55×10^0	kmol kg_{cat}^{-1} h^{-1} atm^{-2}
$E_{a_{11}}$	5.000	kcal mol^{-1}

Consequently, the pseudo-homogeneous model in one dimension is adopted, the mass balance for the *i*-species being:

$$u_s \frac{dC_i}{dz} = \nu_i r \rho_{bed} = \frac{dq_i}{dz} \quad (2)$$

Table 2
System of reactions that take place in the commercial isomerization reactor and their kinetic expressions

Isomerization		
I	*p*-Xylene ⇔ *m*-xylene	$r_I = (k_1 K_p P_p - k_{m1} K_m P_m)/(1 + K_p P_p + K_o P_o + K_m P_m)$
II	*m*-Xylene ⇔ *o*-xylene	$r_{II} = (k_2 K_m P_m - k_{m2} K_o P_o)/(1 + K_p P_p + K_o P_o + K_m P_m)$
Hydrogenolysis		
III	*p*-Xylene + H_2 → toluene + CH_4	$r_{III} = k_3 P_h P_p$
IV	*o*-Xylene + H_2 → toluene + CH_4	$r_{IV} = k_4 P_h P_o$
V	*m*-Xylene + H_2 → toluene + CH_4	$r_V = k_5 P_h P_m$
VII	Ethylbenzene → toluene + CH_4	$r_{VII} = k_7 P_{ebz}$
Ethylbenzene isomerization		
VI	Ethylbenzene → *o*-, *p*-, *m*-xylene	$r_{VI} = k_6 P_{ebz}$
Disproportionation		
VIII	2 *p*-xylene ⇔ toluene + trimethylbenzene	$r_{VIII} = k_8 P_p^2 - k_{m8} P_t P_{tmb}$
IX	2 *o*-xylene ⇔ toluene + trimethylbenzene	$r_{IX} = k_9 P_o^2 - k_{m9} P_t P_{tmb}$
X	2 *m*-xylene ⇔ toluene + trimethylbenzene	$r_X = k_{10} P_m^2 - k_{m10} P_t P_{tmb}$
XI	2 toluene → benzene + *o*-, *p*-, *m*-xylene	$r_{XII} = k_{11} P_t^2$

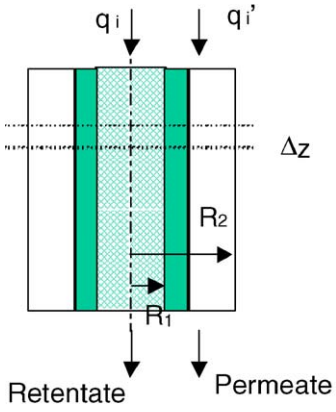

$$\frac{dq_i'}{dz} - \frac{2 \cdot D_i \cdot R_1 \cdot \left(Pi' - Pi\right)}{R_2^2 - R_1^2} = 0$$

$$\frac{dq_i}{dz} + \frac{2 \cdot D_i \cdot \left(P_i' - P_i\right)}{R_1} - \nu_i \cdot r \cdot \rho_{bed} = 0$$

Fig. 1. Membrane reactor configuration and mass balance equations (adapted from reference [20]).

Eq. (2) is an initial value problem, which allows for the simulation of the reactor when the entrance conditions are known.

Since the reactor is adiabatic, it is possible to describe its temperature profile, i.e.:

$$\frac{\mathrm{d}T}{\mathrm{d}z} = f(z) \tag{3}$$

$$u_s \rho_g \, \mathrm{cp}_g \frac{\mathrm{d}T}{\mathrm{d}z} = -\Delta H_{\mathrm{reaction}} \rho_{\mathrm{bed}} r \tag{4}$$

Hence,

$$\frac{\mathrm{d}T}{\mathrm{d}z} = -\frac{\rho_{\mathrm{bed}}}{q_{\mathrm{total}} \, \mathrm{Cp}_g} \Delta H_{\mathrm{reaction}} r \tag{5}$$

This equation complements the mass balance, and is accounted for in the Arrhenius parameters of each reaction.

In order to describe the momentum balance, the pressure drop along the reactor was estimated from Ergun's equation [15]:

$$\frac{\mathrm{d}P}{\mathrm{d}z} = \left[\frac{150(1-\varepsilon)}{D_{\mathrm{part}}} + 1.75G\right] \frac{1-\varepsilon}{\varepsilon^3} \frac{G}{D_{\mathrm{part}} \rho_g} \tag{6}$$

Thus, a complete description of the profiles of pressure, temperature and composition can be obtained.

A fourth-order Runge–Kutta method was used to perform the simulations in Mathcad®. As mentioned above, kinetic parameters taken from the literature were adjusted in order to describe the commercial reactor behavior, using an iteration routine to minimize the sum of errors (between the plant data and the simulations) for the aromatic compounds at the reactor exit.

The error was calculated according to:

$$\mathrm{error} = \left(\frac{\mathrm{output}_{\mathrm{simul}} \, (\mathrm{kg\,h^{-1}})}{\mathrm{output}_{\mathrm{plant}} \, (\mathrm{kg\,h^{-1}})} - 1\right) \times 100 \tag{7}$$

3.3. Membrane reactor modeling

The literature reviewed [16–22] allowed us to select the most adequate model for the case of an isomerization reactor also including a membrane. Kikuchi et al. [18] studied the steam reforming of methane using a computer simulation that compared CVD membranes with electroless-plating Pd membranes on commercial scale. Nam et al. [19] studied the same reaction, analyzing a Pd–Ru membrane reactor. Their model prediction is in good agreement with experimental results. Ito et al. [16] conducted a mathematical analysis to study reaction accompanied by separation, finding better performance with a membrane reactor. Other researchers, such as Ostrowski et al. [17], Prabhu et al. [20] and Jordat et al. [21] also developed models to describe membrane reactors for important processes. The model proposed by Prabhu et al. [20], which is similar to that presented by Wu and Liu [22], is adopted in this work and is slightly modified to take into consideration the reactor geometry.

In case of including the presence of a membrane permeable to the compound of major interest, one of the feasible configurations of the reactor could be described by Fig. 1 [20]. The central region corresponds to the catalyst bed, surrounded by a membrane, and an external zone along which the permeate species flow. The mass balances for each species going through the membrane are modified, adding a term that takes into account the permeation phenomenon.

The species that are assumed to pass the membrane are the three xylene isomers [23]. Both hydrogen and methane are considered not to pass through the membrane because the permeate sweep gas consists mainly of hydrogen and also contains methane, so the flow rate of the sweep gas might be handled industrially so as to keep both partial pressures identical in each side of the membrane. Trimethylbenzene would not be able to flow through the membrane channels due to its dimensions and steric problems. As for the other compounds, the permeances reported by Baertsch et al. [24] were taken into account to carry out trial simulations. These permeances and the actual plant flow rates allowed us to assume that ethylbenzene, toluene and benzene do not pass through the membrane [23].

The partial pressure of each compound can be evaluated at both sides of the membrane. For the retentate side:

$$P_i = y_i P = \frac{Q_i}{\sum_{j=1}^{j=n} Q_j} P \tag{8}$$

whereas for the permeate side, the analogous equation can be used:

$$P_i' = y_i' P' = \frac{Q_i'}{\sum_{j=1}^{j=n'} Q_j'} P' \tag{9}$$

The pressure drop in the retentate side is described by Ergun's Eq. (6), whereas for the permeate side total pressure is assumed constant since the sweep flow is high enough to assure this condition.

The model still assumes a plug-flow pseudo-homogeneous model, so the input conditions are the initial conditions for concentration, pressure and temperature. This can be summed up as follows:

For the retentate side : At $z = 0$,

$$P_i(z) = P_i^0 \quad \text{and} \quad T(z) = T^0 = T^{0'}$$

For the premeate side, at the entrance there only exists sweep gas,

$$\text{so :} \quad \text{At } z = 0, \qquad P_i'(z) = 0 \quad \text{and} \quad T(z) = T^{0'}$$

As shown in the first part of this work, MFI (silicalite and ZSM-5) membranes supported on stainless steel are a potential alternative, because their channels dimensions are comparable to the xylene isomer diameters and they have good performance at various conditions. ZSM-5 membranes have proved to achieve a good separation of *p*-xylene, even at high temperature. Additionally, the constant elimination of this isomer would help to shift the isomerization reaction equilibrium, improving the reaction yield.

In this case, and taking into consideration the industrial conditions, the membranes that could be used in industry should not only be *p*-xylene selective but they also should be able to manage high fluxes [25].

4. Results and discussion

4.1. Plug-flow reactor

Daily information corresponding to one year of reactor operation was provided by the company. Data from several representative days were selected to optimize the kinetic constants in order to obtain a satisfactory fit.

Typical input conditions employed in the simulations are enumerated below—input temperature: 371.6 °C; input pressure: 9.5 atm; molar flow rates (kmol h^{-1}): *p*-xylene, 37.9; *o*-xylene, 53.6; *m*-xylene, 169.6; hydrogen, 2963.3; ethylbenzene, 64.8; benzene, 1.9; toluene, 16.7; methane, 526.5.

The catalyst that is used in the industrial reactor consists of spheres of silica–alumina containing Pt, with a particle diameter of 1.588×10^{-3} m and a surface area of 116 m^2 g^{-1}.

The fits obtained for the commercial plug-flow reactor are shown in Fig. 2. The simulated fitted profiles of the most important compounds are displayed, as well as the plant data acquired both at the input and output of the reactor.

The temperature profiles obtained in the simulations were consistent with plant information. The total temperature difference oscillated between 5 and 12 °C, depending on the operation day analyzed.

The error at the reactor exit was calculated in the case of the compounds shown in Fig. 2, and achieved an acceptable level. It is important to point out that the sum of errors was minimized, and not the individual errors for each compound. The fits led to the errors shown in Table 4.

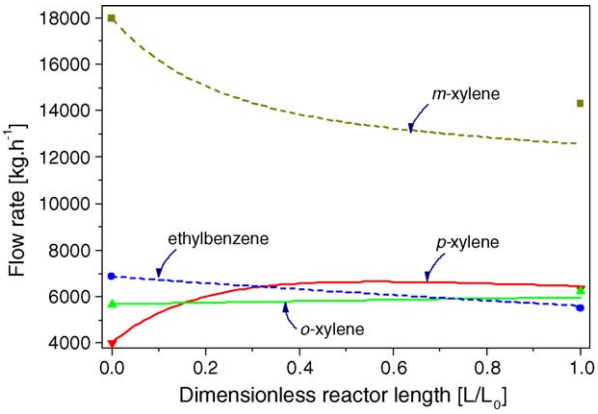

Fig. 2. Commercial isomerization reactor profiles using adjusted kinetic data. Lines: simulation; points: experimental data.

4.2. Membrane reactor

In the first part of this work [26], it has been shown that ZSM-5 membranes, supported on stainless steel tubes, present promising features for the selective separation of xylenes at temperatures as high as 400 °C. The permeation regime is described by a combination of adsorption–diffusion steps whose balance is modified by the introduction of aluminum in the MFI lattice. The permeances for the three xylene isomers through a ZSM-5 membrane were determined in our laboratories at several temperatures. The values used for the simulations correspond to ternary mixtures at 370 °C, and they are: 4.70×10^{-8}, 8.44×10^{-9} and 8.45×10^{-9} mol s^{-1} m^{-2} Pa^{-1} for *p*-, *o*- and *m*-xylene, respectively. The *p*-/*o*-xylene permeation selectivity at this temperature is 5.57, whereas the *p*-/*m*-xylene selectivity is 5.56.

The analysis carried out in the first part of this work in our laboratories indicate that the membrane does not present catalytic activity. This can be attributed to its lack of acidity since it is synthesized from NaZSM-5.

Fig. 3 shows the *p*-xylene profiles along the reactor for the case of:

(a) the plug-flow reactor, without membrane;
(b) a possible configuration of a membrane reactor, considering the permeances presented in the first part of this work for a xylene ternary mixture over a ZSM-5 membrane at 370 °C.

Table 4
Errors in the commercial reactor simulation, with adjusted kinetic data

Compound	Output flow rate error (%) [(output$_{simul}$ (kg h^{-1}))/(output$_{plant}$ (kg h^{-1})) − 1] × 100
p-Xylene	+1.95
o-Xylene	−4.35
m-Xylene	−12.06
Ethylbenzene	+1.90
Toluene	−0.92

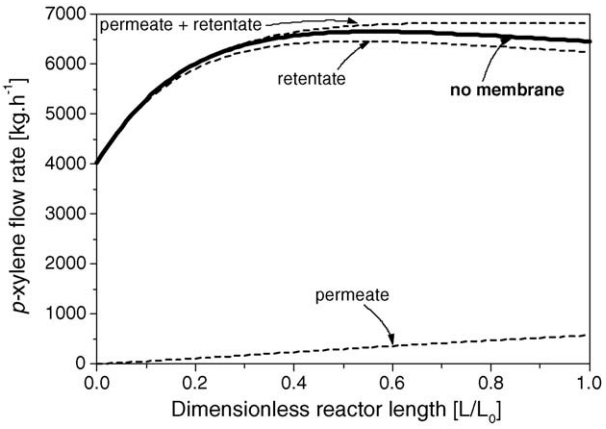

Fig. 3. *p*-Xylene profile for ZSM-5 membrane reactor and commercial reactor. Lines: commercial reactor without membrane; dash: membrane reactor. Ternary mixture permeances obtained at 370 °C. Permeation area: $A_{\text{permeation\_IX}}$. Sweep gas flow rate: 10^5 kmol h^{-1}.

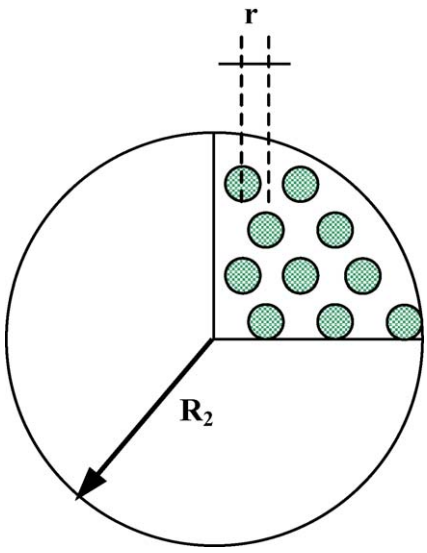

Fig. 4. Transversal view of a membrane reactor with multiple packed tubes.

For the plug-flow reactor, the total pressure drop is 13.2% of its initial value, whereas for the membrane reactor it represents 30.6% of the input value. This difference can be expected since the Ergun Eq. (6) considers the value of the total mass flow "*G*", which is inversely proportional to the section of catalyst. This section is reduced when a set of tubes with membrane is introduced in the original fixed-bed reactor, originating a bigger pressure drop for the same catalyst load. Both the retentate and permeate *p*-xylene profiles are represented in the case of the membrane reactor. The sum of these profiles is also shown so as to demonstrate that this sum is always higher than the commercial reactor performance, indicating that the presence of a membrane enhances the reactor operation. The temperature profile along the reactor is not substantial; therefore, the effective permeabilities of xylenes are regarded as constant in the simulations.

Either for design or optimization purposes, if a bigger permeation area is required, the presence of a set of tubes packed with catalyst can be suggested. Not only would this arrangement lead to a higher *p*-xylene yield but also the current crystallization process could be avoided, bringing about a reduction in the *p*-xylene separation costs. In this case, the equations should be adapted to consider this modification. The equations that describe the membrane reactor include some parameters that could be modified during simulations, among them: permeation area, sweep gas flow rate in the permeate region, permeance of the compounds that pass through the membrane. The manipulation of those variables is performed separately in order to assess their influence on the reactor performance.

4.2.1. Permeation area

The plant reactor is not currently completely filled with catalyst, so the reactor geometry can be changed with relative freedom. The introduction of membrane tubes and their distribution would occupy a given reactor volume, resulting in an increase of the catalyst level for the same load. A set of multiple tubes with membranes appears as an interesting alternative since this would not imply major changes in the existing equipment and, as mentioned before, it would reduce the current costs of *p*-xylene separation. Take, for instance, the scheme in Fig. 4. The following geometric parameters can be defined:

$$\text{Number of tubes}: \quad n \tag{10}$$

$$\text{Total reactor section}: \quad A_{\text{reactor}} = \pi R_2^2 \tag{11}$$

$$\text{Reaction section}: \quad A_{\text{t}} = n\pi r^2 \tag{12}$$

$$\text{Permeate section}: \quad S_{\text{permeate}} = \pi(R_2^2 - nr^2) \tag{13}$$

$$\text{Permeation area}: \quad A_{\text{permeation}} = n(2\pi r L_0) \tag{14}$$

It can be noticed that the bigger the number of present tubes, the higher the permeation area. The radii of those tubes can be as small as necessary, within physical and constructive feasibility, as long as the catalyst bed is homogeneous. It must be pointed out that the catalyst bed offers resistance to the gas flow, generating a pressure drop. Consequently, and for comparative purposes, a constant reaction section is adopted so that the total length of reactor is maintained constant for the different permeation areas assumed for the simulations, thus generating the same total pressure drop along the reactor (ca. 30% of its initial value). In Table 5, a summary of the adopted permeation areas and geometric features of the set of tubes is presented.

Fig. 5 shows the results of using this set of different permeation areas with ZSM-5 membranes. The permeance results obtained in the first part of this work, at 370 °C for ternary mixtures of xylenes, are used in the simulation. It should be highlighted that the entrance temperature of the commercial reactor is ca. 370 °C; therefore, the simulations with data at this temperature reflect the plant conditions accurately.

Fig. 5 also shows that the bigger the permeation area, the better performance of the reactor.

Taking the adopted permeation area A_X as a representative value that introduces a significant improvement in the reactor, its performance can be depicted by the following information—input ratio (kg h^{-1}): *p*-/*o*-/*m*-xylene

Table 5
Permeation areas adopted for the simulations

Denomination	Number of tubes n	Radius of each tube r (m)	Total bed height L_0 (m)	Permeation area (m^2)
$A_{permeation\_I}$	100	0.157	2.50	247.3
$A_{permeation\_II}$	200	0.111	2.50	349.7
$A_{permeation\_III}$	500	0.070	2.50	552.9
$A_{permeation\_IV}$	1000	0.0498	2.50	781.9
$A_{permeation\_V}$	2000	0.035	2.50	1105. 8
$A_{permeation\_VI}$	3000	0.029	2.50	1354.3
$A_{permeation\_VII}$	5000	0.022	2.50	1748.4
$A_{permeation\_VIII}$	10000	0.0157	2.50	2472.6
$A_{permeation\_IX}$	15000	0.0128	2.50	3028.4
$A_{permeation\_X}$[a]	99115	0.005	2.50	7784.5

[a] This area was estimated considering the dimensions of the tubes used in the first part of this work [26].

is 4018.352/5672.707/17973.846, which is normalized with respect to *p*-xylene is 1.000/1.412/4.473.

Analyzing the output of the plug-flow and the membrane reactor, the same ratio can be compared so as to note the improvement introduced by the membrane in the *p*-xylene yield.

For the output of the plug-flow reactor the ratio takes the following figures (kg h^{-1}): *p*-/*o*-/*m*-xylene is 6365.69/5961.189/12349.12, which represents 1.000/0.936/1.940.

Considering the output of the retentate side on the one hand: *p*-/*o*-/*m*-xylene is 5795.77/5724.23/11766.80 (kg h^{-1}), normalized is 1.000/0.988/2.030. On the other hand, the exit of the permeate side results (kg h^{-1}): *p*-/*o*-/*m*-xylene is 1396.919/247.393/595.089, which equals 1.000/0.177/0.426. Adding both contributions (permeate + retentate) the output ratio is (kg h^{-1}): *p*-/*o*-/*m*-xylene is 7192.689/5971.622/12361.89, which normalized gives 1.000/0.830/1.719.

The analysis of these figures allows us to conclude that the mixture is enriched in *p*-xylene at the exit of the plug-flow reactor. Moreover, for the membrane reactor, the sum of both permeate and retentate side at the output shows that the amount of *p*-xylene is bigger than in the case of the conventional fixed-bed catalytic reactor introducing an improvement in *p*-xylene yield.

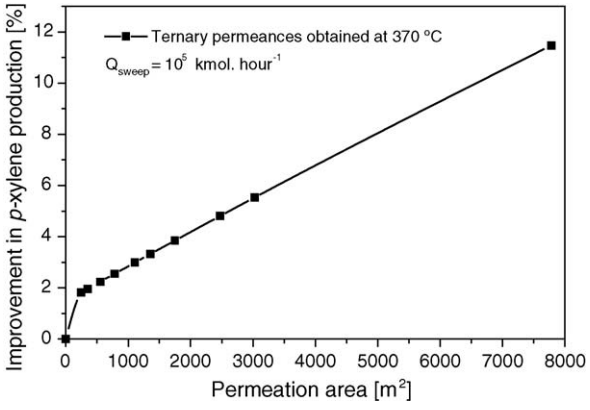

Fig. 5. Influence of the permeation area in the production of *p*-xylene, compared to the commercial reactor, for xylene permeances obtained at 370 °C.

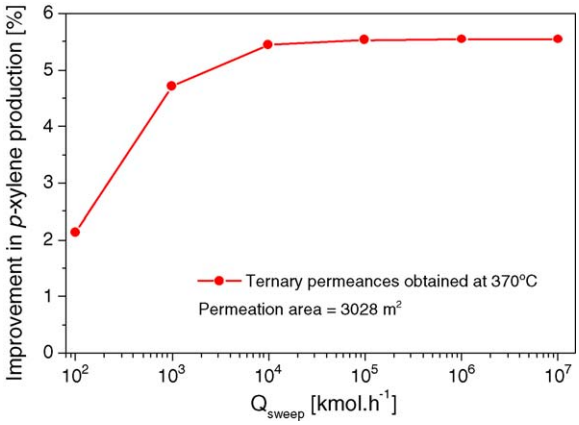

Fig. 6. Influence of the sweep gas flow rate in the production of *p*-xylene, compared to the commercial reactor, for xylene permeances obtained at 370 °C.

4.2.2. Sweep gas flow rate

This variable can be reasonably modified since an excess of H_2 is available in the plant, and this gas can be used both as sweep and carrier for the xylenes. From the partial pressure equation:

$$P_i' = \frac{Q_i'}{\sum Q_i' + Q_{sweep}} P' \quad (15)$$

It can be noticed that if the sweep gas flow rate is increased, the partial pressure of the desired compound decreases. Consequently, the driving force for permeation is augmented if P_i' is small or, ideally null.

Fig. 6 shows the membrane reactor performance for different values of sweep gas flow rate. The reactor performance improves when this parameter is increased. In addition, it can be observed that there is an asymptote from a sweep gas flow rate of 10^5 kmol h^{-1}. This value is assumed as the optimum since the movement of bigger amounts of H_2 would not result in much more performance enhancement and it would represent higher pumping costs.

4.2.3. Permeance of xylenes

Some exploratory simulations are proposed considering an increase in the effective permeability of *p*-xylene, assuming constant the ones for the other isomers. In our laboratory, efforts are directed to improving membrane performance; thus, it is foreseeable that better permeabilities and *p*-xylene selectivities will be obtained in the future. Fig. 7 shows the increase in the *p*-xylene production when its permeance is augmented up to 50% of the present value measured at 370 °C, while those of *m*-xylene and *o*-xylene are kept constant. In Fig. 7a it can be observed that the maximum of *p*-xylene in the reactor side is shifted to lower values of reactor length when *p*-xylene permeation increases, whereas the opposite occurs if the contribution of the sweep gas side is taken into account (Fig. 7b). As a result, a linear increase in *p*-xylene production is observed in Fig. 7c. This result encourages more research efforts towards improving membrane selectivity.

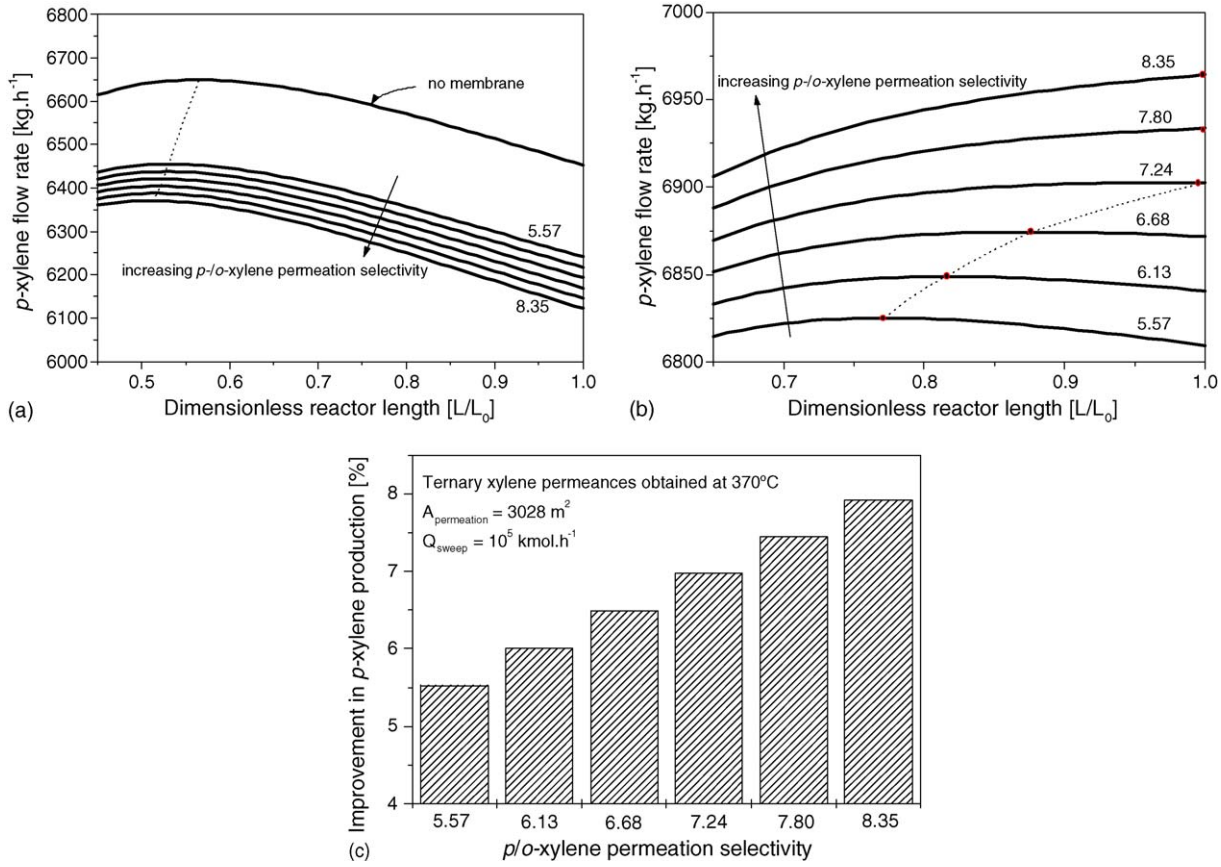

Fig. 7. Influence of the *p*-/*o*-xylene permeation selectivity in the production of *p*-xylene. (a) Retentate side *p*-xylene profiles, (dash) line that shows how the maximum is shifted; (b) (retentate + permeate) *p*-xylene profiles, (dash) line that shows how the maximum is shifted; (c) improvement in *p*-xylene production.

5. Conclusion

A set of kinetic parameters was optimized in order to simulate the behavior of an industrial reactor. The plug-flow conventional model was modified by adding a ZSM-5 membrane supported on SS tubes, which was developed in our laboratory. Simulation results predict that increases in *p*-xylene production as high as 12% can be achieved while maintaining the pressure drop in reasonable practical values (30.6% of the input value) and tubes within physical and constructive feasibility. Under these restrictions, the performance of the membrane reactor can be optimized by increasing permeation area from 0 to 8000 m^2 and sweep gas flow rate from 10^2 to 10^5 kmol h^{-1}. Under this conditions, while the output of the conventional plug-flow reactor gives a ratio *p*-/*o*-/*m*-xylene of 1.000/0.936/1.940, in the case of the membrane reactor the rate is improved to 1.000/0.830/1.719, considering both the permeate and retentate side contributions. However, better *p*-xylene permeation selectivities are desirable; to this end, research efforts are already under way in our laboratories.

Acknowledgements

The authors wish to acknowledge the financial support received from UNL, CONICET and ANPCyT. Thanks are given to Elsa Grimaldi for the English language editing. A. Deshayes thanks the YPF Foundation for the support received for her scholarship.

References

[1] J. Caro, M. Noack, P. Kölsch, R. Schäfer, Micropor. Mesopor. Mater. 38 (2000) 3–24.
[2] J.N. Armor, Appl. Catal. A: Gen. 49 (1) (1989) 1–25.
[3] G. Xomeritakis, S. Nair, M. Tsapatsis, Micropor. Mesopor. Mater. 38 (2000) 61–73.
[4] M. Tsapatsis, G. Xomeritakis, H. Hillhouse, S. Nair, V. Nikolakis, G. Bonilla, Z. Lai, Cattech 3 (2) (2000) 148–163.
[5] O. Cappellazo, G. Cao, G. Messina, M. Morbidelli, Ind. Eng. Chem. Res. 30 (1991) 2280–2287.
[6] A. Corma, A. Cortés, Proceedings of the V Simposio Iberoamericano de Catálisis, 1976, pp. 309–312.
[7] A. Cortés, A. Corma, J. Catal. 51 (1978) 338–344.
[8] A. Corma, A. Cortés, I. Nebot, F. Tomas, J. Catal. 57 (1979) 444–449.
[9] A. Corma, A. Cortés, Ind. Eng. Chem. Process Des. Dev. 19 (1980) 263–267.
[10] K.L. Hanson, A.J. Engel, AIChE J. 13 (2) (1967) 260–266.
[11] S. Bhatia, S. Chandra, T. Das, Ind. Eng. Chem. Res. 28 (1989) 1185–1190.
[12] G.F. Froment, K.B. Bischoff, John Wiley and Sons Inc., 1979.
[13] G.F. Froment, Ind. Eng. Chem. 59 (2) (1968) 18–27.
[14] J.J. Carberry, McGraw-Hill Chem. Eng. Series, 1976.
[15] R.B. Bird, W.E. Stewart, E.N. Lightfoot, Wiley, New York, 1960.
[16] N. Ito, Y. Shindo, K. Haraya, K. Obata, T. Hakuta, H. Yoshitome, Int. Eng. Chem. 25 (1) (1985) 138–142.

[17] T. Ostrowski, A. Giroir-Fendler, C. Mirodatos, L. Mleczko, Catal. Today 40 (1998) 181–190.
[18] E. Kikuchi, I. Nemoto, M. Kajiwara, S. Uemiya, T. Kojima, Catal. Today 56 (2000) 75–81.
[19] S.W. Nam, S.P. Yoon, H.Y. Ha, S. Hong, A.P. Maganyuk, Korean J. Chem. Eng. 17 (3) (2000) 288–291.
[20] K. Prabhu, A. Liu, L.G. Lovell, S.T. Oyama, J. Membr. Sci. 177 (2000) 83–95.
[21] K. Jordal, R. Bredesen, H.M. Kvamsdal, O. Bolland, Energy 29 (2004) 1269–1278.
[22] J.C.S. Wu, P.K.T. Liu, Ind. Eng. Chem. Res. 31 (1992) 322–327.
[23] A. Deshayes, M.Sc. Thesis, Universidad Nacional del Litoral, 2003.
[24] C.D. Baertsch, H.H. Funke, J.L. Falconer, R.D. Noble, J. Phys. Chem. 100 (1996) 7676–7679.
[25] J. Hedlund, J. Sterte, M. Anthonis, A.J. Bons, B. Carstensen, N. Corcoran, D. Cox, H. Deckman, W. De Gijnst, P.P. de Moor, F. Lai, J. McHenry, W. Mortier, J. Reinoso, J. Peters, Micropor. Mesopor. Mater. 52 (2002) 179–189.
[26] A. Tarditi, S. Irusta, E. Lombardo, Chem. Eng. J. 122 (2006) 167–174.